J Electr Eng Technol.2016; 11(4): 860-868
http://dx.doi.org/10.5370/JEET.2016.11.4.860

ISSN(Print) 1975-0102
ISSN(Online) 2093-7423

A 3 kW Bidirectional DC-DC Converter for Electric Vehicles

Arsalan Ansari*, Puyang Cheng* and Hee-Jun Kim†

Abstract – A bidirectional DC-DC converter (BDC) is an indispensable electrical unit for the electric vehicles (EVs). High efficiency, high power density, isolation, light weight and reliability are all essential requirements for BDC. In this paper, a 3 kW BDC for the battery charger of EVs is proposed. The proposed converter consists of a half-bridge structure on the primary side and an isolation transformer and a synchronous rectifier structure on the secondary side. With this topology, minimum number of switching devices are required for bidirectional power flow between the two dc buses of EVs. The easy implementation of the synchronous rectification gives advantages in terms of efficiency, cost and flexibility. The proposed BDC achieves high efficiency when operating in both modes (step-up and step-down). A 3 kW prototype is implemented to verify theoretical analysis and the performance of the proposed converter.

Keywords: Bidirectional DC-DC converter, Battery charger, Electric vehicles, Efficiency

1. Introduction

With the global energy crisis the conventional vehicles (internal combustion engines) face the increasingly serious problems of energy. In contrast, the EVs especially battery electric vehicles (BEVs) depend on variety of options for its driving power. BEVs offer the advantages of safety, silent operation and no emissions when powered by renewable energy sources such as wind or solar which are virtually emission free [1]. These vehicles can also make efficient use of energy by storing energy recovered during braking or deceleration cycle in the batteries. The storage or charging process of the battery is achieved by a BDC, which is the key block in EV energy system to link high voltage (HV) dc bus and low voltage (LV) dc bus as shown in Fig. 1. This BDC should have high power density and high efficiency to meet the desired goals for EV's battery charger. When the EV is parked, the battery can be charged by the household utility outlet from the grid through the BDC. For the other case when the EV is in the driving state, the BDC provides the electrical power from LV battery to the motor through DC-AC inverter and also DC loads in the EV.

BDCs are broadly classified into isolated and non-isolated types. The conventional non-isolated buck/boost BDC cannot operate in the wide voltage conversion range [2]. The isolated BDC are preferred for EVs due to the advantages of high voltage conversion ratio and safety. Many different types of isolated BDCs [3-6] have been proposed due to these advantages, some full-bridge BDCs

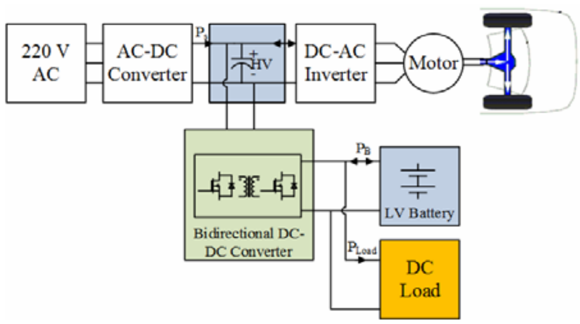

Fig. 1. The energy system of EV

[7-10] have also been proposed in recent years. However, full-bridge converters have the disadvantage of high voltage ripples if not employing an extra voltage clamping circuit [11]. By contrast, half-bridge converters [12-14] have a simple structure and a better anti-imbalance ability in the transformer. In some topologies of half-bridge converters, MOSFET body diodes are applied for synchronous rectification in both buck/boost modes [15], but high conduction losses result in low efficiency, thus limiting the use of these converters to only low power applications.

This paper describes the development of a 3 kW BDC for EVs. The converter consists of a half-bridge topology, an isolation transformer and a synchronous rectifier. The isolation transformer provides the advantages of wide conversion range and safety, and the easy implementation of synchronous rectification offers the benefits in terms of efficiency, cost and flexibility. However, this structure has been mostly proposed for less than 1.5 kW application [3, 11-13, 16-17], so the operation of more than 3 kW in both step-up and step-down modes has the practical significance for the EV battery charger products.

† Corresponding Author: Dept. of Electronic Systems Engineering, Hanyang University, Korea. (hjkim@hanyang.ac.kr)
* Dept. of Electronic Systems Engineering, Hanyang University, Korea. (arsalan.07el@gmail.com, chengpuyang@outlook.com)
Received: June 9, 2015; Accepted: October 29, 2015

2. Topology Configuration and Operational Principles

2.1 Topology configuration

Fig. 2 shows the circuit diagram of the proposed half-bridge BDC. The design uses a half-bridge connected with the DC power supply on the primary side and a center-tapped transformer and a synchronous rectification on the secondary side. The converter can operate in two modes, namely, step-down mode and step-up mode. All of the four switches Q_1–Q_4 are gated in both modes. Switch Q_1 is complementary with switch Q_4, and switch Q_2 is complementary with switch Q_3.

In the step-down mode, the primary side DC power supply V_H (210–380 V) charges the secondary side battery V_L (21–29 V), and Q_3 and Q_4 provide rectification. In contrast, Q_1 and Q_2 operate as rectifiers in the step-up mode when V_L supplies the high side battery V_H. For mathematical insight into the proposed converter, some assumptions are made as: (i) the ON-state resistance $R_{DS(ON)}$ of all switches is ignored; (ii) the capacitors C_1, C_2 and C_o are large enough, and the voltage across the capacitors can be taken as constant; and (iii) the capacitance of the capacitors C_1 and C_2 is equal i.e. $C_1 = C_2 = C$. Thus, $V_{C1} = V_{C2} = V_H/2$; and (iv) $D_1 - D_4$ are the body diodes of $Q_1 - Q_4$, and the diode forward resistance is zero.

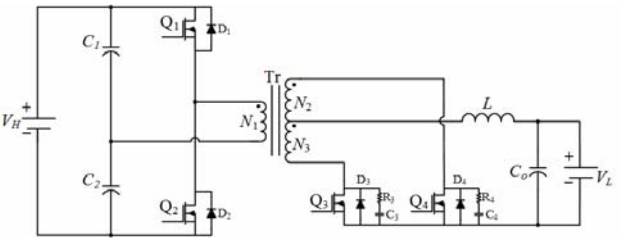

Fig. 2. Circuit diagram of the proposed converter

2.2 Operational principles of the proposed BDC

2.2.1 Step-down mode

This is similar to a buck converter operational mode in which V_H supplies V_L with the charging current, i_L. The equivalent circuits are shown in Fig. 3. The pulse-width modulation (PWM) technique is used to control the switches Q_1–Q_4. In both modes Q_1 and Q_2 are gated, with the duty cycle less than 0.5, while the duty cycle of Q_3 and Q_4 is more than 0.5. Fig. 4 shows some typical waveforms for the step-down mode. The operating principles during one switching period are described as follows:

Stage 1 [t_0–t_1]: Switch Q_1 turns on and switch Q_4 turns off at t_0, while switch Q_3 remains on. The current flow path for this stage is shown in Fig. 3(a). In this stage $v_{AB}=V_H/2$, the current i_1 flows through Q_1 as i_p, which is reflected from inductor current i_L. The current i_L increases linearly and flows totally through switch Q_3 to charge the battery

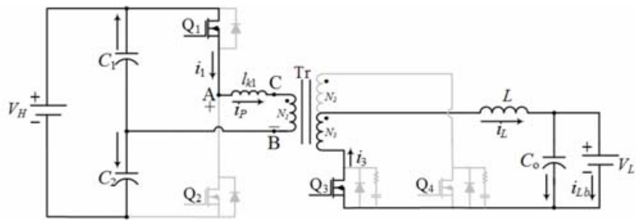

(a) Stage 1

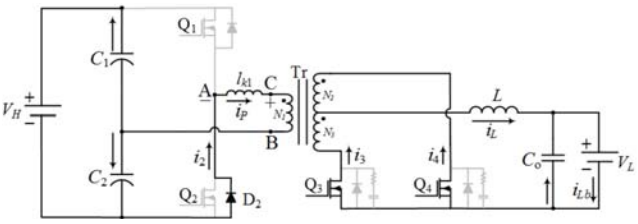

(b) Stage 2

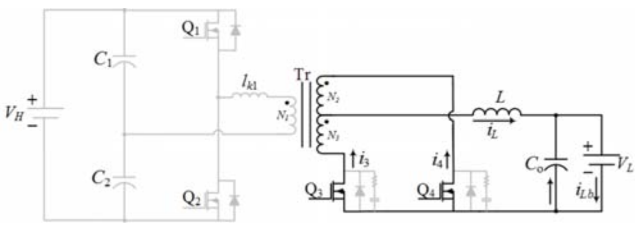

(c) Stage 3

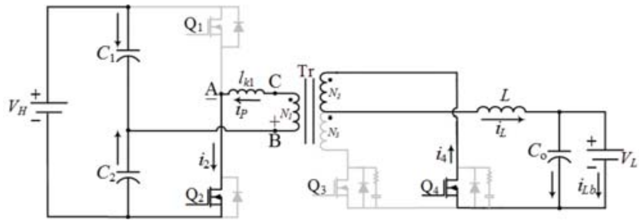

(d) Stage 4

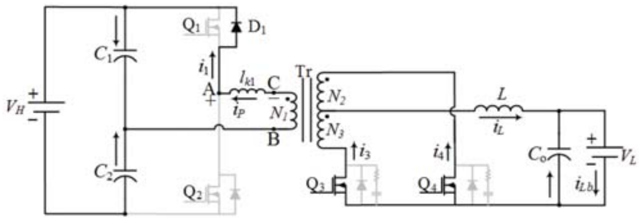

(e) Stage 5

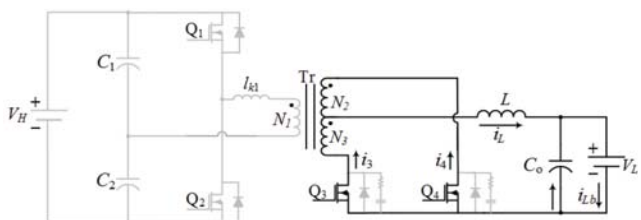

(f) Stage 6

Fig. 3. Equivalent circuits for the step-down mode

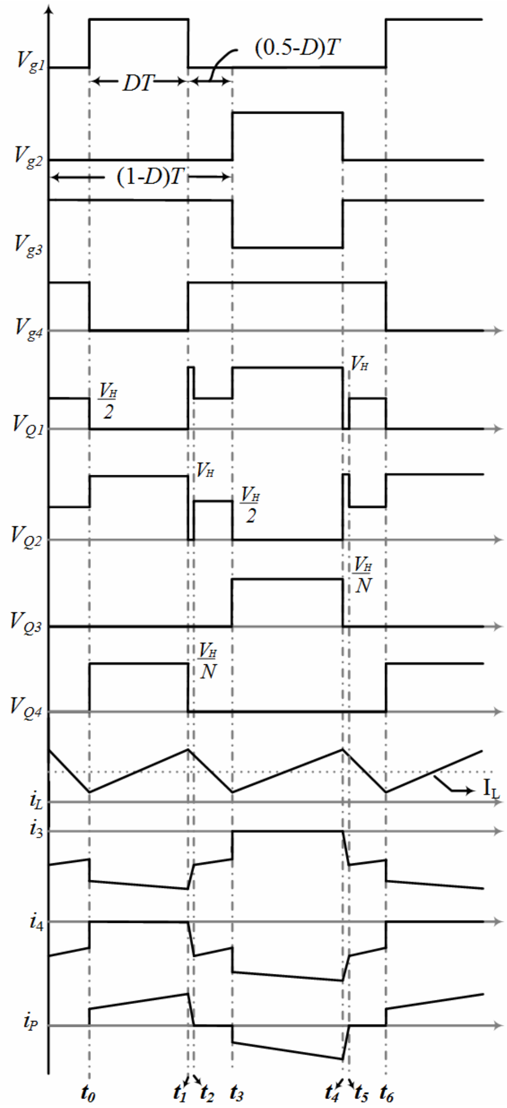

Fig. 4. Theoretical waveforms for the step-down mode

V_L.

Stage 2 [t_1–t_2]: Switch Q_1 turns off and switch Q_4 turns on at t_1, while switch Q_3 still remains on. Because of the transformer leakage inductance l_{k1}, there is freewheeling current through D_2 [Fig. 3(b)], $v_{CA}=V_H/2$ and i_p decreases linearly to zero. In this stage v_A is clamped to ground so $v_{Q2}=0$ and $v_{Q1}=V_H$. Meanwhile i_4 increases and i_3 decreases linearly and at t_2, $i_3=i_4=i_L/2$.

Stage 3 [t_2–t_3]: Switch Q_1 and Q_2 are in off state and $v_{Q1}=v_{Q2}=V_H/2$. In this stage, $v_{AB}=0$, no power is transferred to secondary side and the energy stored in the inductor L charges the low side battery V_L [Fig. 3(c)]. The current i_L is shared equally by switches Q_3 and Q_4.

Stage 4 [t_3–t_4]: Switch Q_2 turns on and switch Q_3 turns off at t_3, while switch Q_4 remains on. The current flow path is shown in Fig. 3(d). This is a similar operation to stage 1[t_0-t_1], but the voltage $v_{AB}=-V_H/2$. The current i_2 is built as $-i_p$. In this stage, Q_4 is conducting and i_4 increases linearly as i_L.

Stage 5 [t_4–t_5]: Switch Q_2 turns off and switch Q_3 turns on at t_4. Switch Q_4 still remains on. Because of l_{k1}, D_1 conducts and v_A is clamped as V_H, therefore $v_{Q2}=V_H$ and $v_{Q1}=0$ [Fig. 3(e)]. Meanwhile i_3 increases and i_4 decreases linearly and at t_5, $i_3=i_4=i_L/2$.

Stage 6 [t_5–t_6]: The operation of this stage is the same as stage 3. The current path for this stage is shown in Fig. 3(f).

2.2.2 Step-up mode

For the step-up mode, the equivalent circuits considering the leakage inductance of the proposed converter are shown in Fig. 5. In this operational mode, V_L discharges to supply the primary side output voltage of V_H with current i_1 or i_2. Because of the existence of the transformer secondary side leakage inductance l_{k2} and l_{k3}, there will be current stress on Q_3 and Q_4. For protection of Q_3 and Q_4, the RC snubber circuit is necessary in parallel connection with Q_3 and Q_4. The theoretical waveforms are shown in Fig. 6, and modes of operation in one period (t_0–t_6) are described as follows:

Stage 1 [t_0–t_1]: Switch Q_3 is turned on at t_0, with switch Q_4 remaining on while Q_1 and Q_2 are in the off state. The current flow path for this stage is shown in Fig. 5(a). The secondary side of the transformer is effectively shorted, and $v_{AB}=0$. Meanwhile, the energy is stored in the inductor L, while no energy is transferred to the primary side. In this stage, i_L increases linearly and is divided equally between Q_3 and Q_4. The primary side battery V_H is charged by the capacitors C_1 and C_2.

Stage 2 [t_1–t_2]: Switch Q_4 is turned off while switch Q_1 is turned on at t_1, with switch Q_3 remaining on. Because of the leakage inductance l_{k2}, there is stress on Q_4 and the RC snubber is charged by i_4 [Fig. 5(b)]. The current i_4 decreases linearly to zero and i_3 increases linearly to i_L, building i_1 as i_p which increases linearly.

Stage 3 [t_2–t_3]: In this stage $v_{AB}=0$ [Fig. 5(c)], the energy stored in L is transferred to the primary side, i_L and decrease in linearity. The capacitor C_2 is discharged and capacitor C_1 is charged.

Stage 4 [t_3–t_4]: Switch Q_4 is turned on, with switch Q_3 remaining on while switch Q_1 is turned off at t_3. This stage is similar to stage 1 in which the inductor L stores energy again, and the inductor current i_L is equally shared by switches Q_3 and Q_4 [Fig. 5(d)]. Capacitor C_1 and C_2 discharge to supply the primary side DC source V_H.

Stage 5 [t_4–t_5]: At t_4 Switch Q_3 is turned off, with switch Q_2 turned on and switch Q_4 remaining on. Because of the leakage inductance l_{k3} [Fig. 5(e)], there is stress on Q_3 and the RC snubber is charged by i_3. The current i_3 decreases linearly to zero with i_4 increasing linearly to i_L, building i_1 as $-i_p$.

Stage 6 [t_5–t_6]: In this stage [Fig. 5(f)], i_4 is built as i_L which decreases in linearity and energy is transferred to primary side. The capacitor C_2 is charged by i_2 conducted by Q_2, which decreases linearly.

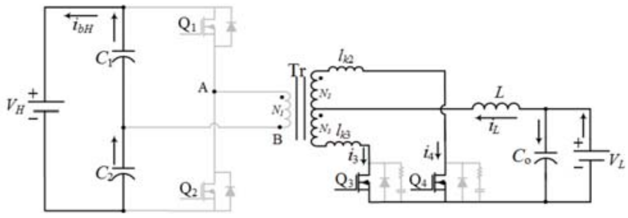

(a) Stage 1

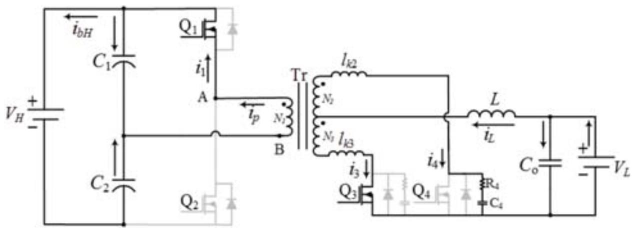

(b) Stage 2

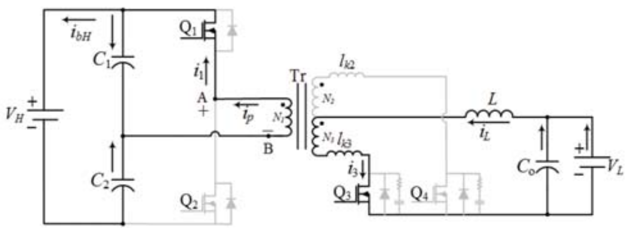

(c) Stage 3

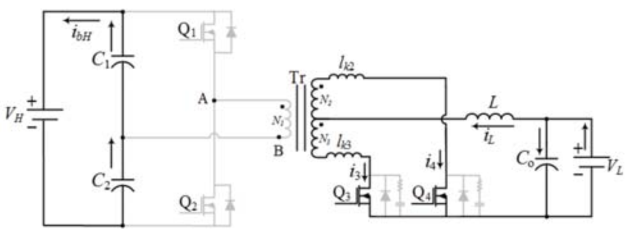

(d) Stage 4

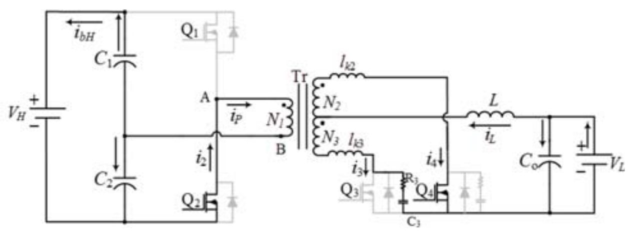

(e) Stage 5

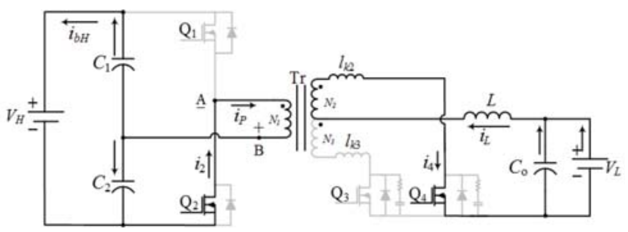

(f) Stage 6

Fig. 5. Equivalent circuits for the step-up mode

3. Circuit Design Analysis

The BDC operates in step-down and step-up modes. Design parameters for the step-down mode will be discussed in detail. The parameters obtained can be used for step-up mode as well. The theoretical analysis and design guidelines will be discussed in this section.

3.1 Step-down mode

When the number of turns on the secondary windings are equal, that is, N_2=N_3, then N can be defined as the transformer turns ratio, as N_1/N_2 or N_1/N_3. The relationship between V_H and V_L is expressed as:

$$V_L = \frac{D \cdot V_H}{N} \tag{1}$$

where D is the duty ratio of Q_1 and Q_2.

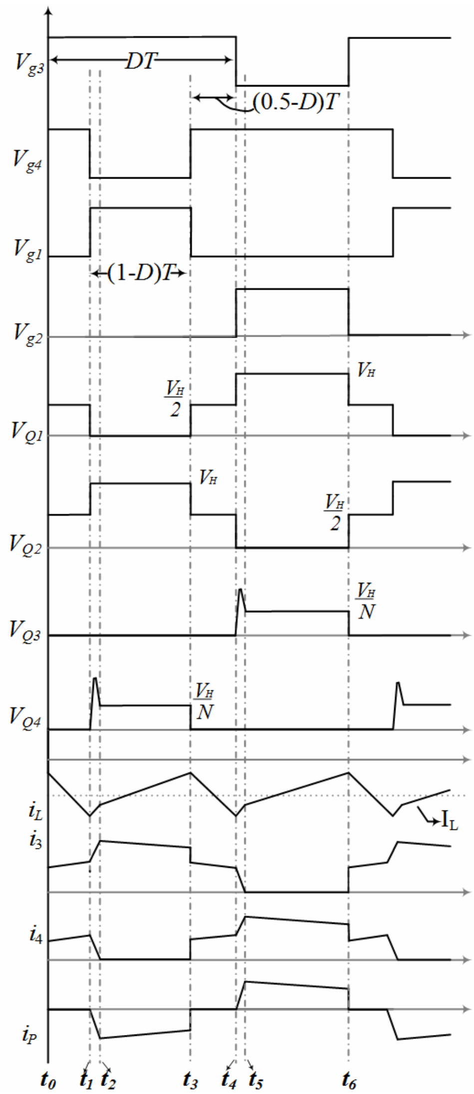

Fig. 6. Theoretical waveforms of the step-up mode

To design the inductor L, the inductor current ripple Δi_L and the minimum duty ratio D_{min} should be considered. The inductance L can be calculated as:

$$L \geq \frac{(0.5 - D_{min}) \cdot V_L}{\Delta i_L f_s} \tag{2}$$

When designing output capacitor C_o, the transient overshoot should be taken into account. Because of the inductor L, the energy stored in L will be transferred to C_o if there is a sudden change of load, causing a sudden change of V_{Co}. According to the design specification, the overshoot voltage should be less than 3% of V_L, so that for a 50% to full load situation, C_o can be calculated as:

$$C_o \geq \frac{V_L (0.5 - D_{min}) T_S^2}{8L\Delta v_{c_o}} \tag{3}$$

and for the equivalent series resistance (ESR) of C_o, the value of ESR should be limited by the following equation:

$$R_{ESR} \leq \frac{\Delta v_{c_o}}{\Delta i_{c_o}} \tag{4}$$

So several capacitors may be connected in parallel, if necessary, to meet the requirements of ESR.

The two capacitors C_1 and C_2 should be large enough to constrain the input current ripple and equally share V_H for Q_1 and Q_2.

In practical applications, there are many reasons causing the voltage imbalance. A few of those are: 1) the conduction periods of the two high side switches Q_1 and Q_2 are not strictly equal, 2) C_1 and C_2 are charged and discharged in turns, and if the capacitance value is not big enough, there will be big voltage ripple which may cause voltage imbalance.

To avoid the voltage imbalance, it is necessary to keep the equal conduction periods for Q_1 and Q_2 to the maximum possibility, and it should be noted that the switch Q_4 is complementary with Q_1 and it is the same situation for Q_2 and Q_3. For C_1 and C_2, there is

$$dv = i_p \frac{dt}{C} \tag{5}$$

where i_p is the transformer primary side current.

It can be seen that if C is big enough, the ripple will be small and it will not affect the circuit operations.

The maximum voltage stress and RMS/max current ratings should be considered when selecting the switches of both sides. Q_1 and Q_2 have the ratings of:

$$\mathrm{V}_{DS(peak)} = \mathrm{V}_H \tag{6}$$

$$I_{RMS} = \frac{I_L \cdot \sqrt{2D}}{N} \tag{7}$$

$$I_{max} = \frac{I_{L(max)}}{N} \tag{8}$$

Q_3 and Q_4 have the ratings of:

$$V_{DSpeak} = \frac{V_H}{N} \tag{9}$$

$$I_{RMS} = [I^2{}_b \cdot D + \left(\frac{I^2{}_b}{2}\right)^2 \cdot (1 - 2D)]^{1/2} \tag{10}$$

$$I_{max} = I_{L(max)} \tag{11}$$

3.2 Step-up mode

For this mode, V_L is the input voltage, and V_H is output voltage. Therefore:

$$V_H = \frac{N \cdot V_L}{1 - D'} \tag{12}$$

where D' is the duty ratio of Q_3 and Q_4.

Because the BDC operates just as the current flows inversely, but the voltage polarity remains unchanged, so the design parameters of all components of step-down mode can be employed in the step-up mode.

4. Experimental Results

A 3 kW prototype, as shown in Fig. 7, was built and tested to evaluate the performance of the proposed BDC. The experimental parameters and circuit components are given in Table 1. The experimental waveforms of step-down and step-up modes are shown in Fig. 8 to Fig. 13.

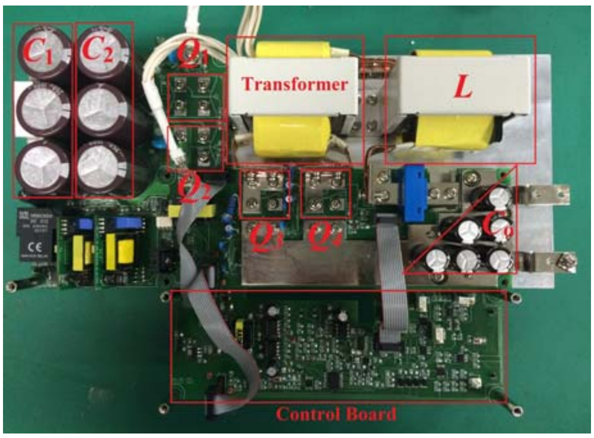

Fig. 7. Detailed photograph of the 3 kW proposed BDC

Fig. 8 shows the voltage across two switches Q_1 and Q_4, which is V_{Q1} and V_{Q4}, respectively, and the input and the output voltage V_H of 380 V and V_L of 29.6 V at light load. One can see that the voltage stress on switch Q_1 is equal to V_H, and that on switch Q_4 is equal to V_H/N. The output voltage V_L is well regulated at 29 V. In this situation, the duty ratio of switches Q_1 and Q_2 is 23.4%.

Fig. 9 shows the inductor current i_L and the switch

Table. 1. Experimental parameters

Parameters	Value
C_1 & C_2	1000uF/250 V × 3 in parallel
C_o	1000 µF/50 V × 6 in parallel
Q_1 & Q_2	IXFN60N80P
Q_3 & Q_4	IXFN210N30P3
L	10 µH
Switching Frequency	50 kHz
Max: Output Power	3 kW
R_3,R_4	8 Ω
C_3,C_4	103 k/1 kV
Transformer para:	
N_1	7.5
N_2 & N_3	2.5
l_{k1}/l_{m1}	28 µH/0.5 mH= 0.56%
l_{k2} or l_{k3}/l_{m2} or l_{m3}	1.2 µH/55 µH= 2.1%

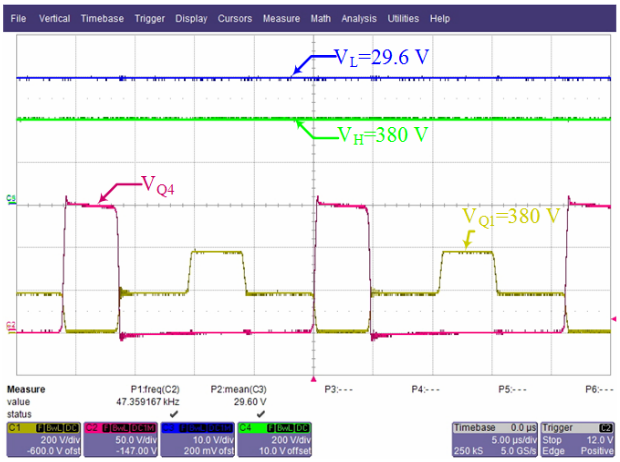

Fig. 8. Step-down mode experimental waveforms at light load

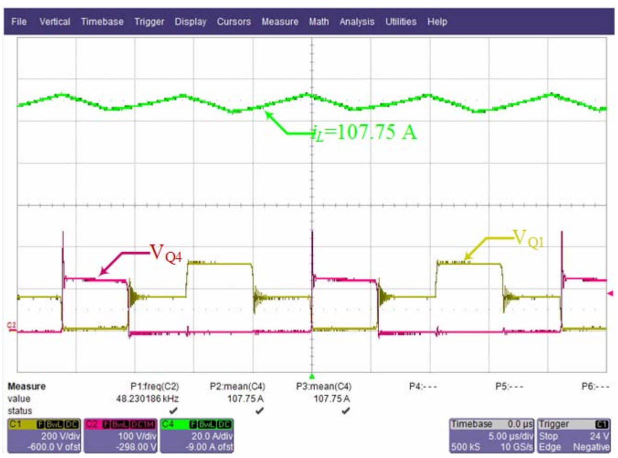

Fig. 9. Step-down mode experimental waveforms at full load

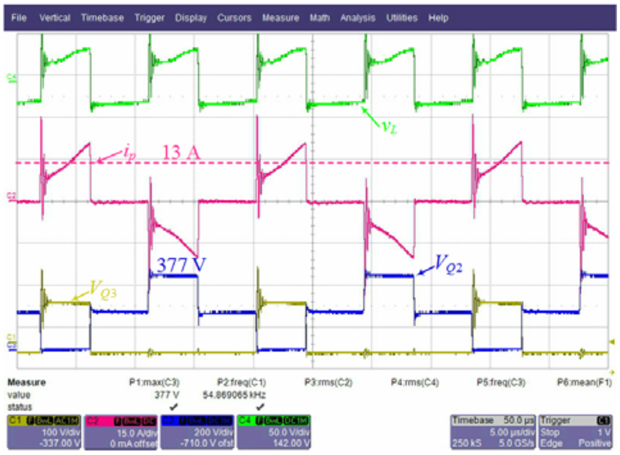

Fig. 10. Step-down mode experimental waveforms at 1 kW

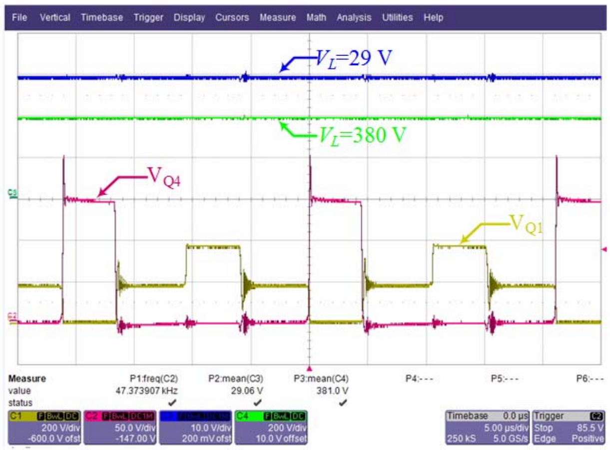

Fig. 11. Step-up mode experimental waveforms at light load

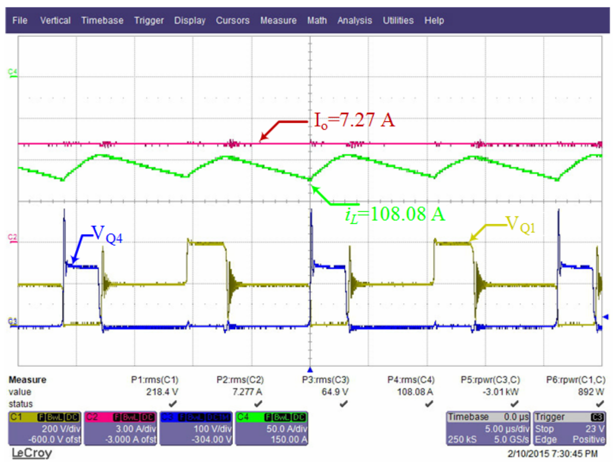

Fig. 12. Step-up mode experimental waveforms at full load

voltages V_{Q1} and V_{Q4} at full load. It can be seen that the average output current $i_{L,Avg}$ is 107.75 A, achieving 3.1 kW output power.

Fig. 10 shows the step-down 1 kW experimental waveforms. Channel 1 and channel 3 show the drain-to-source voltage V_{Q3} and V_{Q2}. The input voltage can be seen from the maximum value of $V_{Q2(\max)}$ as 377 V and the output voltage is 29 V. In this situation the duty ratio of Q_1 and Q_2 is about 23.1%. Channel 2 shows transformer primary side current which changes the direction accordingly when Q_1 or Q_2 are turned on. The average value of every conduction period is about 13 A. Channel 4 shows the voltage across L.

Fig. 11 shows V_{Q1}, V_{Q4}, V_L and V_H for the step-up mode at light loads. It should be noted that the output voltage is well regulated at 380 V, and the maximum voltage on switch Q_1 is equal to V_H and that on switch Q_4 is V_H/N. In this situation, the duty ratio of Q_3 and Q_4 is 77.2%.

Fig. 12 shows the average input current of -108.08 A, output current of 7.26 A, and the voltage across switches Q_1 and Q_4 at full load conditions. The input and output power obtained are 3.13 kW and 2.76 kW, respectively.

Fig. 13 shows the step up mode 2 kW experimental waveforms. The input voltage is 29 V and the output voltage can be seen from $V_{Q2(max)}$ as 351 V. In this situation the duty ratio of Q3 and Q4 is about 75.2%. Channel 2 shows transformer primary side current i_P with the average value of every conduction period about 23 A. Channel 4 shows the voltage across the inductor L.

Fig. 14 shows the measured efficiencies of the proposed BDC when it operates in step-down mode. The converter achieves efficiency of higher than 90% from 30% to full load.

Fig. 15 shows the measured efficiencies of the proposed converter when it operates in step-up mode. It can be seen that more than 88% of the efficiency is achieved from 30% to full load.

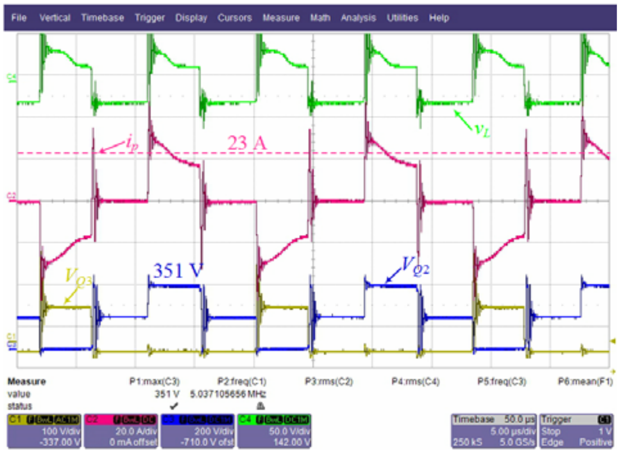

Fig. 13. Step-up mode experimental waveforms at 2 kW

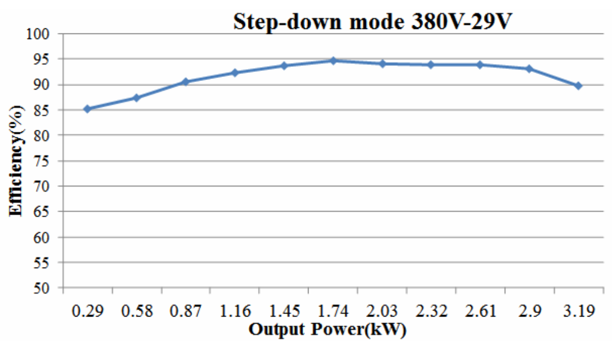

Fig. 14. System efficiency in step-down mode

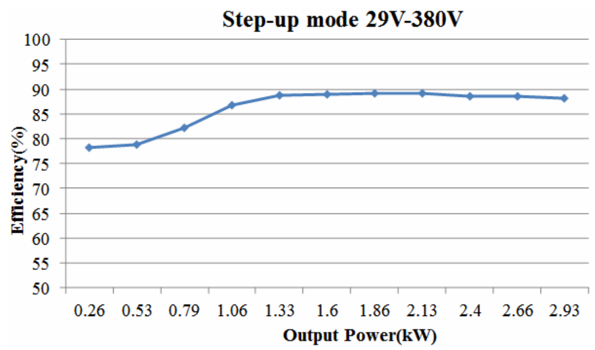

Fig. 15. System efficiency in step-up mode

5. Conclusion

A 3 kW BDC for EVs is proposed in this paper. With a simple topology structure, the converter consists of a half-bridge on the primary side and a synchronous rectifier on the secondary side. Four switches are employed in both the step-down mode and step-up mode. The theoretical analyses have been proved by the experimental results of the 3 kW prototype circuit. When operating in step-down mode, an efficiency was achieved of more than 90% from 30% to the full load, while an efficiency of 88.2% is achieved at full load for the step-up mode.

Acknowledgments

This work was supported by the Human Resources Program in Energy Technology of the Korea Institute of Energy Technology Evaluation and Planning (KETEP), granted financial resources from the Ministry of Trade, Industry and Energy, Republic of Korea. (20154030200730)

This work was supported by the Energy Efficiency & Resources Department of the Korea Institute of Energy Technology Evaluation and Planning (KETEP) and was granted financial resources from the Ministry of Trade, Industry and Energy, Republic of Korea. (20132010101950)

References

[1] Junsung Park, and Sewan Choi, “Design and control of a bidirectional resonant DC-DC converter for automotive engine/battery hybrid power generators,” *IEEE Transactions on Power Electronics*, vol. 29, no. 7, pp. 3748-3757, 2014.

[2] C.C. Lin, L.S. Yang and G.W. Wu, “Study of a non-isolated bidirectional DC-dc converter,” *IET Power Electronics*, vol. 6, no. 1, pp. 30-37, 2013.

[3] Z. Zhang, O. Thomsen, and M. Andersen, “Optimal design of a push-pull-forward half-bridge (PPFHB) bidirectional DC-DC converter with variable input voltage,” *IEEE Trans. Industrial Electron*ics, vol. 59, no. 7, pp. 2761-2771, 2012.

[4] F. Zhang and Y. Yan, “Novel forward-flyback hybrid bidirectional DC-DC converter,” *IEEE Transactions on Industrial Electronics*, vol. 56, no. 5, pp. 1578-1584, 2009.

[5] Gang Chen, Yim-Shu Lee, S. Y. R. Hui, Dehong Xu, and Yousheng Wang, “Actively clamped bidirectional flyback converter,” *IEEE Transactions on Industrial Electronics*, vol. 47, no. 4, pp. 770-779, 2000.

[6] K. Venkatesan, “Current mode controlled bidirectional flyback converter,” *in proceedings of 20th Annual IEEE Power Electronics Specialists Conference, PESC*, pp. 835-842, 1989.

[7] K. Wu, C. de Silva, and W. Dunford, “Stability analysis of isolated bidirectional dual active full-bridge DC-DC converter with triple phase-shift control,” *IEEE Transactions on Power Electronics*, vol. 27, no. 4, pp. 2007-2017, 2012.

[8] R. Naayagi, A. Forsyth, and R. Shuttleworth, “High-power bidirectional DC-DC converter for aerospace applications,” *IEEE Transactions on Power Electronics*, vol. 27, no. 11, pp. 4366-4379, 2012.

[9] C. Zhao, S. Round, and J. Kolar, “Full-order averaging modelling of zero-voltage-switching phase-shift bidi-rectional DC-DC converters,” *IET Power Electronics*, vol. 3, no. 3, pp. 400-410, 2010.

[10] C. Mi, H. Bai, C. Wang, and S. Gargies, “Operation, design and control of dual H-bridge-based isolated bidirectional DC-DC converter,” *IET Power Electronics*, vol. 1, no. 4, pp. 507-517, 2008.

[11] S. Park, and Y. Song, “An interleaved half-bridge bidirectional DC-DC converter for energy storage system applications,” *in proceedings of 8th IEEE International Conference on Power Electronics and ECCE Asia (ICPE & ECCE)*, pp. 2029-2034, 2011.

[12] B.-R. Lin, C.-L. Huang, and Y.-E. Lee, “Asymmetrical pulse width modulation bidirectional DC-DC converter,” *IET Power Electronics*, vol. 1, no. 3, pp. 336-347, 2008.

[13] F. Peng, H. Li, G.-J. Su, and J. Lawler, “A new ZVS bidirectional DC-DC converter for fuel cell and battery appli-cation,” *IEEE Transactions on Power Electronics*, vol. 19, no. 1, pp. 54-65, 2004.

[14] H. Li, F. Z. Peng, and J. Lawler, “A natural ZVS medium-power bidirectional DC-DC converter with minimum number of devices,” *IEEE Transactions on Industry Applications*, vol. 39, no. 2, pp. 525-535, 2003.

[15] M. Jain, P. Jain, and M. Daniele, “A bidirectional DC-DC converter topology for low power application,” *in proceedings of 28th Annual IEEE Power Electronics Specialists Conference, PESC* vol. 1, pp. 804-810, 1997.

[16] João Silvestre, “Half-bridge bidirectional DC-DC Converter for small Electric Vehicle.” *IEEE International Symposium on Power Electronics, Electrical Drives, Automation and Motion, SPEEDAM,* 2008.

[17] Zhiyong Ma, and Renjie Hu. “Zero-voltage-switching condition of isolated-type symmetrical half-bridge bidirectional DC/DC converter.” *in proceedings of IEEE International Conference on Electrical and Control Engineering (ICECE),* 2011.

Arsalan Ansari received his B.E. degree in electrical engineering from the Mehran University of Engineering and Technology, Jamshoro, Pakistan, in 2011. He is currently moving towards the completion of his Ph.D. degree in electrical engineering at Hanyang University, Ansan, Korea. He was appointed as a Lecturer with Mehran University of Engineering and Technology. His current research interests include bidirectional DC-DC converters, multilevel inverters and grid-connected renewable energy systems. Mr. Ansari was a recipient of the Scholarship for the Integrated Master and Ph.D. Program by the Government of Pakistan. He was a medalist among his engineering batch.

Puyang Cheng received his B.S. degree in Mechanical Engineering and Automation from Wuhan University of Science and Technology, Wuhan, China, in 2013. He is currently working toward the M.S. degree in Electrical Engineering in Hanyang University, Ansan, Korea. His research interests are bidirectional DC/DC converters and power factor correction.

Hee-Jun Kim received the B.S and M.S. degree in electronics engineering from Hanyang University, Seoul, Korea, in 1976 and 1978, respectively, and the Ph.D. degree from Kyushu University, Fukuoka, Japan, in 1986, all in electronics engineering. Since 1987, he has been a Professor with Hanyang University, Ansan, Korea. His current research interests include switching power converters, soft-switching techniques, and analog signal processing. Prof. Kim is a senior member of IEEE.